

Wrench related faults and their control on the tectonics and Eocene sedimentation in the L13–L15 sub-sag area, Pearl River Mouth basin, China

Shuping Chen¹ · Shunshan Xu² · Yu Cai³ · Xiaodan Ma⁴

Received: 5 January 2017 / Accepted: 14 July 2017 / Published online: 18 September 2017
© Springer Science+Business Media B.V. 2017

Abstract Recent oil discoveries in the L13–L15 sub-sag area in the Pearl River Mouth basin have inspired interest in Paleogene hydrocarbon targets. However, the structures and their control on reservoirs have not been completely studied. The aim of this paper is to address the tectonics and Eocene sedimentation based on 3D seismic data. We documented characteristics from four aspects of the faults in the study area: (a) fault arrangement; (b) fault segmentation; (c) flower structures; and (d) distribution of the depocenters along the faults. Based on the above data, we propose that the structures in the studied area were formed by a right-handed wrench. The principal shear for this model was caused by NNE- to NE-ward motion of the eastern part of the Eurasia plate due to the collision of the Indian–Australian and Eurasian plates starting approximately 49 Ma ago. The L13–L15 sub-sag area underwent early Eocene rifting, a late Eocene rifting–depression transition and an Oligocene–Quaternary thermal depression. The rift phase included three stages: the initial rifting, intensive rifting and late rifting. The deep lake mudstone deposited during the intensive rifting stage is the source rock with the most potential for oil generation. Shallow lake source rocks formed in the late rifting and transition

stages are the secondary source rocks. Reservoir sweet spots were formed in the early period of the intensive rifting and late rifting stages. The junction sites between the front of the meandering river delta plain and fault steps are favorable places for good reservoirs. The sediments in the transition stage are rich in sandstone, making them perfect sites for prospecting reservoirs.

Keywords Pearl River Mouth basin · Wrench · Tectonics · Sedimentology · Petroleum geology

Introduction

The various trending faults in the Paleogene system in the Pearl River Mouth basin (PRMB) make it difficult to understand the basin's dynamics. They also blur the understanding of the ways in which source rocks and reservoirs occur. The L13–L15 sub-sag area is one part of the Zhu-1 depression in the PRMB (Fig. 1). Further analysis of the geotectonic conditions will aid in understanding the formation and evolution of the PRMB and will contribute to oil exploration in the basin.

The PRMB is rich in oil and gas (Yang 2000; Shi et al. 2009). There are two petroleum systems in the basin. The source rocks of the lower petroleum system are related to the deep lake mudstone in the Wenchang formation and the source rocks of the upper petroleum system are shallow lake mudstones in the Wenchang and Enping formations (Fig. 2). The former is the main source rock in the basin and has a large thickness, wide distribution area, and high maturity. It is in a peak hydrocarbon expulsion period at present. The latter provides oil and gas in local areas with a limited distribution area.

✉ Shuping Chen
csp21c@163.com

¹ State Key Laboratory of Petroleum Resources and Prospecting, China University of Petroleum, Beijing 102249, China

² Centro de Geociencias, Universidad Nacional Autónoma de México, Apartado Postal 1-742, 76001 Querétaro, Qro., Mexico

³ Daqing Oilfield Limited Corporation, PetroChina, Daqing 163513, Heilongjiang, China

⁴ Tarim Oilfield Company, PetroChina, Korla 841000, Xinjiang, China

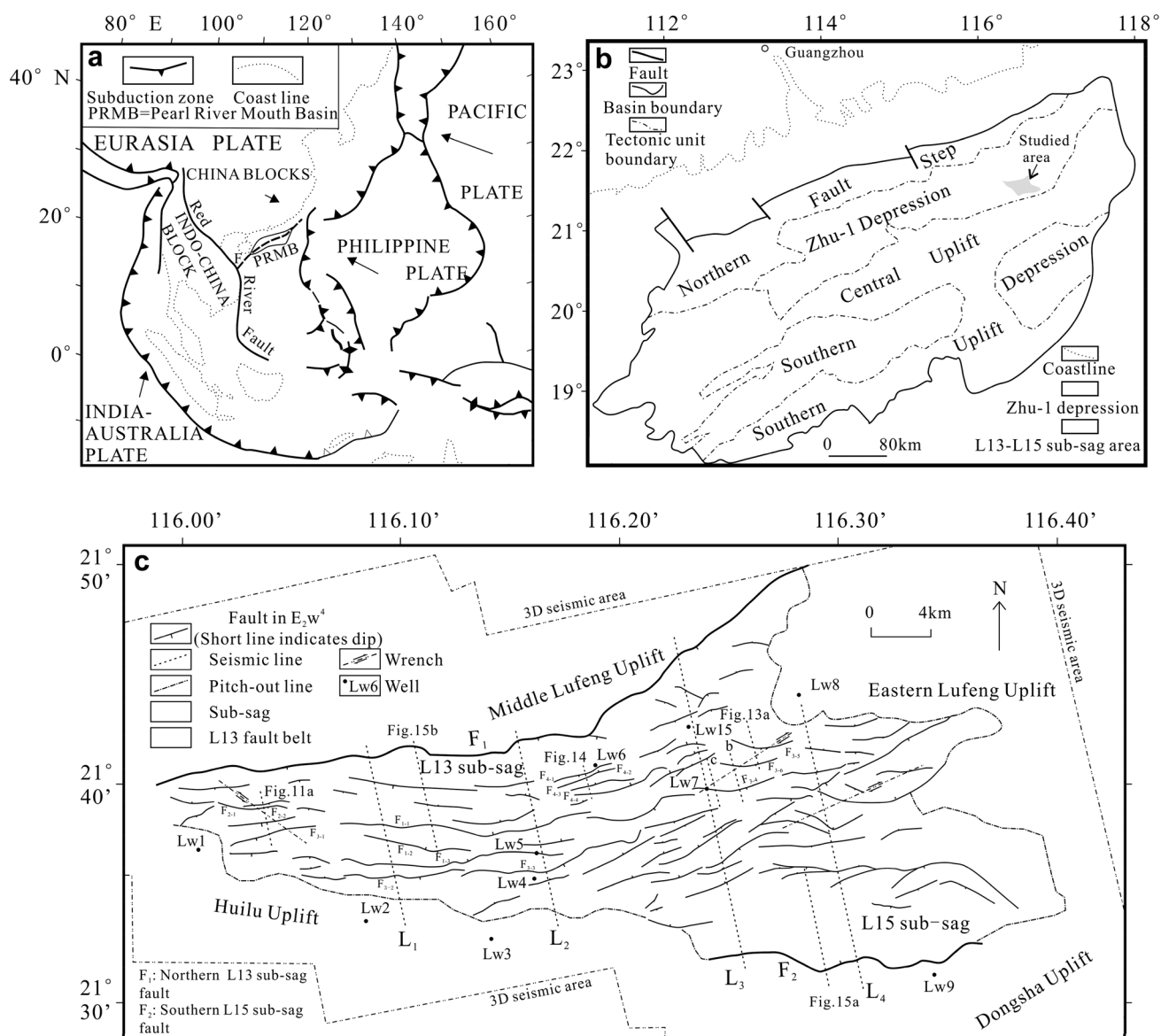


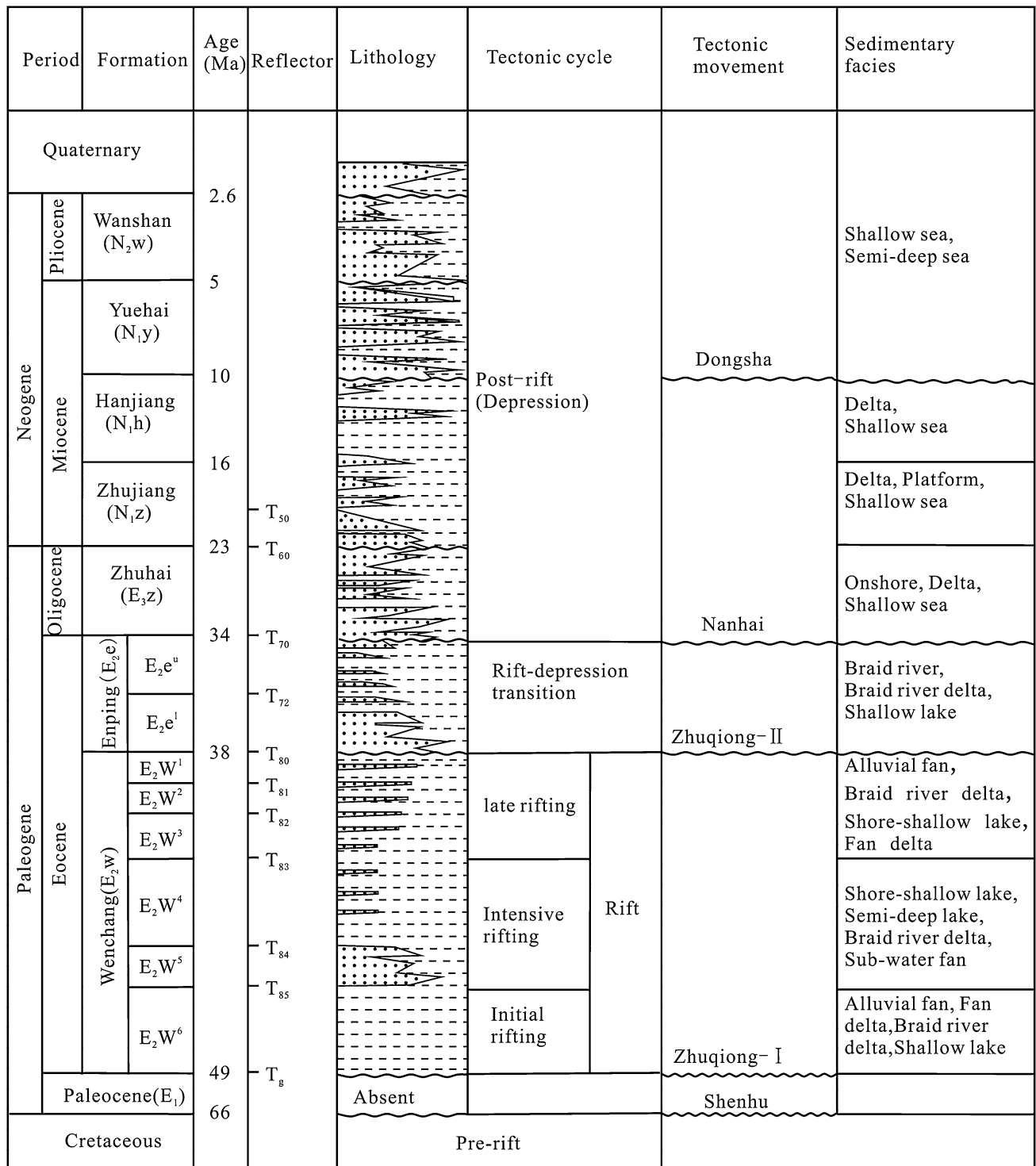
Fig. 1 Tectonic maps of the L13–L15 sub-sag area: **a** plate tectonics; **b** tectonic units of the Pearl River Mouth basin; **c** structural map of the L13–L15 sub-sag area. **a** and **b** are modified from Honza and

Fujioka (2004) and Zhu et al. (2015). F is the Qiongdongnan fault (Li et al. 2012) or Yuedong fault (Xu and Zhang 1999)

Petroleum exploration has shown that the Neogene system of the Zhu-1 depression contains more than 90% of the oil and gas discoveries in the basin (Shi 2013). The Zhu-1 depression is at the northern part of the PRMB and is divided into five sags like those of the Lufeng and Hanjiang sags.

The recent oil discovery in the L13 fault belt presently includes Paleogene targets (Fig. 1b, c) (Shu et al. 2014; Zhu et al. 2015), especially the Wenchang and Enping Formations (Fig. 2). However, the distribution of good reservoirs has not been well studied. To make the distribution clearer, it is essential to further study and understand the tectonics.

In this study, we focus on the structural characteristics and dynamics of the L13–L15 sub-sag area based on 3D seismic data. At the same time, we will also provide some insights on the tectonics of the Zhu-1 depression. The control of tectonics on deposition will be discussed as well. The result of this paper will provide new data on the formation of the Pearl River Mouth basin and the South China Sea.



Legend: [Dotted pattern] Sandstone [Dashed pattern] Mudstone

Fig. 2 Sedimentary strata and evolutionary stages in the L13–L15 sub-sag area. E₂w⁶: sixth member of the Wenchang formation (E₂w). E₂w⁵: fifth member of the Wenchang formation (E₂w). E₂w⁴: fourth member of the Wenchang formation (E₂w). E₂w³: third member of

the Wenchang formation (E₂w). E₂w²: second member of the Wenchang formation (E₂w). E₂w¹: first member of the Wenchang formation (E₂w). E₂e^l: lower section of the Enping formation (E₂e). E₂e^u: upper section of the Enping formation (E₂e)

Geological setting

The PRMB is located in the connection area among the Pacific plate, the Eurasian plate and Indian–Australian plate (Fig. 1a). The formation and evolution of the PRMB resulted from both the subduction of the Pacific plate beneath the Eurasian plate and the collision between the Indian–Australian plate and the Eurasian plate in the Cenozoic. The basement of the PRMB is composed of Precambrian crystal rocks and is a part of the Cathaysia block, with Caledonic and late Mesozoic fold belts (Sun et al. 2014). The rocks are mainly Mesozoic sandstones, mudstones, volcanic rocks and granite and some Sinian-Lower Paleozoic shallow metamorphic sandstones and conglomerates (Sun et al. 2014). The basin can be divided into two uplifts and two depressions (Fig. 1b). The Zhu-1 depression, which has a total resource amount of 53×10^8 t, is the part of the PRMB with the most potential for oil reserves (Shi 2013). The northern part of the Zhu-1 depression consists of two uplifts and two sags, among which is the Lufeng sag (Fig. 3). The L13–15 sub-sag area is located at the southeast part of the Lufeng sag along wells Lw1 and Lw5. This area is composed of the L13 sub-sag, L13-fault belt and L15 sub-sag.

The basin filling in the L13–L15 sub-sag area is composed of Eocene, Oligocene, Neogene and Quaternary sediments (Fig. 2). Eocene sedimentary rocks are characterized by continental facies including fan delta, meandering river, shore-shallow lake and deep lake with sandstone, siltstone and mudstone sediments. Volcanic rocks occur in the Eocene base. The sediments from the Oligocene to the present are those of the Zhuhai, Zhujiang, Hanjiang, Yuehai and Wanshan formations and the Quaternary. The Sedimentary facies are marine facies, and the rocks include sandstone, siltstone and mudstone.

Methodology

In the study area, 1800 km² 3D seismic data covering the entire study area were collected and processed by the Shenzhen Branch, CNOOC (China) Ltd. in 2003, 2005, 2007, 2010 and 2014. The seismic data were processed using 3D PreStack Depth Migration (PSDM). The PSDM seismic data were displayed in the time domain to accommodate previous data that were displayed in the time domain. There are 18 wells, two of which penetrated through the Wenchang formation, nine of which penetrated into the Wenchang

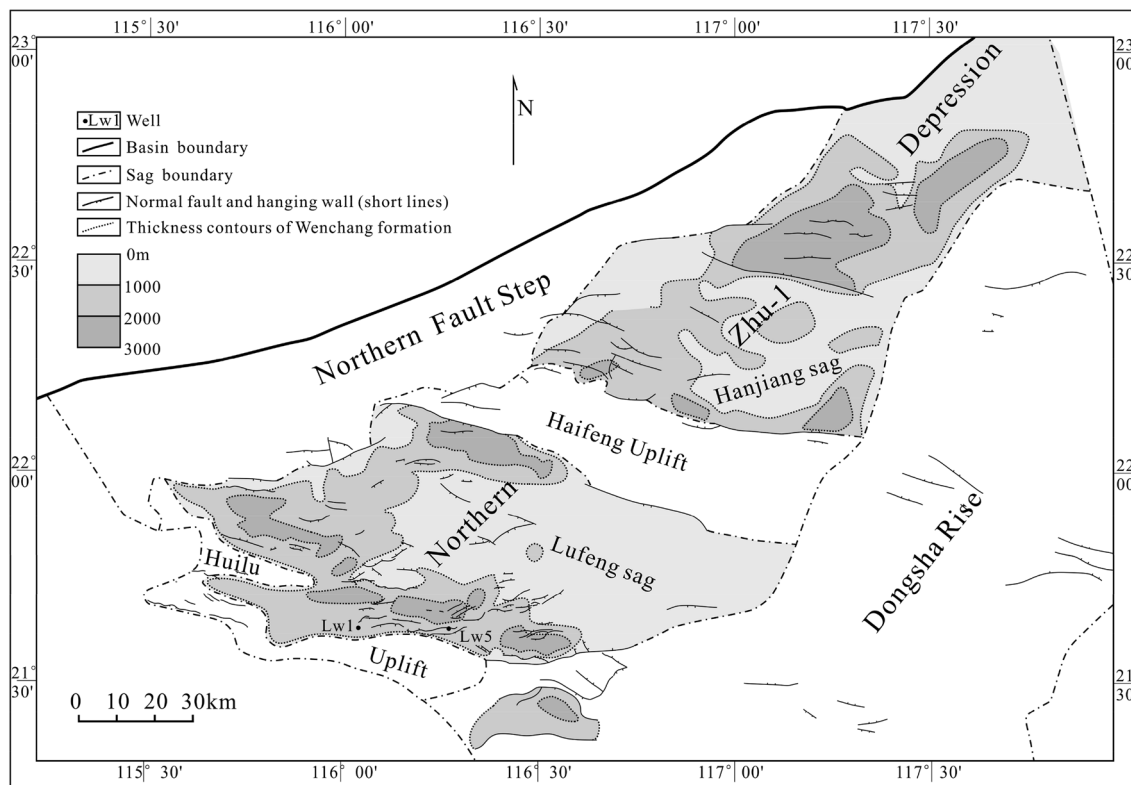


Fig. 3 Tectonic units of the northern Zhu-1 depression. The boundaries between the sags and uplifts are in the NWW strike direction. They are slopes and faults. The faults and thickness contours are in

NWW, NEE and NE strike directions and are nearly parallel to the boundary faults, suggesting that the faults controlled the distribution of the sediments during the Wenchang Period

formation, and seven of which penetrated into the Enping formation. Conventional logging was performed for 12 Wells. The well cores for the Wenchang and Enping formations were obtained from eight wells.

The quality of the 3D seismic was analyzed. In the Enping formation, the dominant frequency was 35 Hz, with a frequency width of 25–48.33 Hz. The best vertical resolution was 27.1 m, and the reasonable vertical resolution range was 19.7–38 m. In the upper section of the Wenchang formation, the dominant frequency was 27.08 Hz, with a frequency width of 5.83–43.33 Hz. The best vertical resolution was 38.8 m. In the lower section of the Wenchang formation, the dominant frequency was 23.33 Hz, with a frequency width of 7.92–33.75 Hz. The best vertical resolution was 45 m.

The horizons were calibrated using both seismic features and well-logging data such as stratum stratification and curves. Some of the horizons were calibrated from adjacent areas. The interpretation of the 3D seismic data was conducted using the Geoframe software. In this study, 11 horizons were picked on a 10 × 20 line and trace grid. The horizons were local unconformities with truncations in the underlying reflectors and overlaps in overlying reflectors.

The balanced cross section method was used in the structural interpretation (Rowan and Kligfield 1989). The layer-along variance volume slices were applied to determine faults in the maps (Zhou et al. 2006). Based on the seismic wave velocity field and time to depth conversion, the cross sections in time and stratum thickness maps in time were used to develop cross sections in meters and stratum thicknesses in meters. The extension amounts and comparisons of the thicknesses of a stratum in the hanging walls to the thickness of a geochronologically identical stratum in the footwalls were used to indicate fault activities (Tearpock and Bischke 1991). The back-stripping technique (Allen and Allen 2013) was applied to the analysis of tectonic evolution. The dynamics of the faults were deduced in terms of the faults assemblage types and plate tectonics (Twiss and Moores 2007).

The sedimentary facies were determined using a correlation plate between the seismic facies and sedimentary facies (Fig. 4). The plate was established based on the calibration of the well data to the seismic facies.

Structural frame work

The L13–L15 sub-sag area comprises the L13 sub-sag, L13 fault belt, and L15 sub-sag (Fig. 1b, c). The L13 sub-sag is located at the northwest of the study area (Fig. 1c). It is a half graben (Figs. 5, 6) or graben (Fig. 7). Its north margin is bounded by the northern L13 sub-sag fault (F_1) and is

near the middle Lufeng uplift to the north. Faults or slopes bound its south margin to the L13 fault belt. The L15 sub-sag is located at the southeast of the L13–L15 sub-sag area and is a half graben (Figs. 1c, 7, 8). Its southern margin is bounded by the southern L15 sub-sag fault (F_2) and is near the Dongsha uplift. Its northern margin is bounded by faults or slopes to the L13 fault belt. The sub-sags and faults trend nearly NWW and NE-NEE, respectively (Fig. 1c). These subsags and faults controlled the thickness contours of the Wenchang Formation (Figs. 3, 9).

Wrench related faults

Fault orientation

Riedel shear patterns are commonly observed in wrench fault systems (Tchalenko 1970). Basins related to Riedel shear are also documented in different tectonic settings in both continental and oceanic crust and occur on a wide range of scales (e.g., Xu et al. 2017). This means that the Riedel shear pattern can be applied to large-scale fault patterns (e.g., Cunningham and Mann 2007). R shears, which are synthetic shears at angles of approximately 15° to the principal shear (Fig. 10b), are generally the first occurring subsidiary fractures and have angles of approximately $\alpha/2$ to the principal displacement zone direction. R' shears are antithetic faults oriented at high angles (approximately 75° , $90 - \alpha/2$) and are conjugate with the R shears (Fig. 10b). They may develop with or after R shears (Moore and Byerlee 1992). The R and R' fractures intersect at acute angles of $90^\circ - \alpha$, where α is the angle of internal friction (Riedel 1929). In some cases, T fractures (tension fractures) oriented at an angle of 45° to the principal displacement zone form during the first stage of wrenching (Davis et al. 2000; Cho et al. 2008; Chen et al. 2010).

Most of the faults in the study area are normal faults with planar, listric (concave), or convex fault surfaces. The faults strikes are in NWW, NE, and NEE directions (Fig. 1c). The dip angles of the faults range from 40° to 60° . A rose diagram of fault orientation (Fig. 10a) indicates two peak orientations (NE 56° and NW 277°) and one sub-peak (NE 77°). These faults match faults related to a NE right-handed wrench (Fig. 10b). The fault group with a peak orientation of NW 277° would be composed partly of T fractures and R' shears together. The fault group with a sub-peak orientation of NE 77° would be composed of secondary T fractures. The fault group with a peak orientation of NE 56° would be composed of R shears.

The northern boundary fault (northern L13 sub-sag fault F_1) in the study area is oriented EW in the western part. The southern boundary fault (southern L15 sub-sag fault F_2) is also oriented EW. The orientations of the two boundary

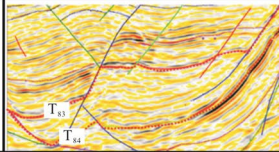
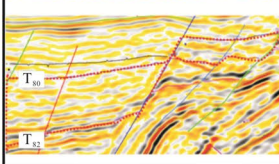
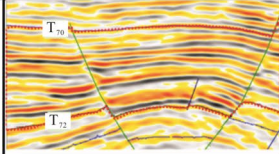
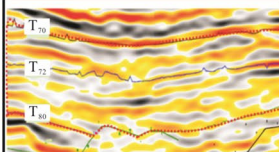
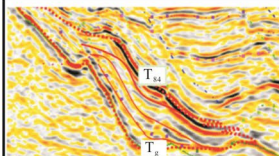
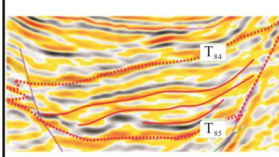
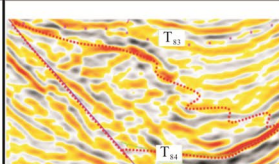
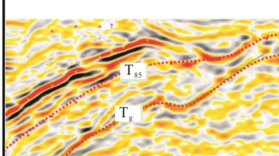
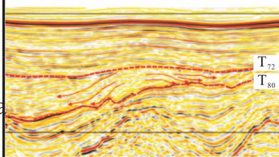
Seismic facies					Sedimentary facies	Seismic profile
	Frequency	Amplitude	Continuity	Configuration		
Sheet seismic facies	Low	Medium-weak	Medium	Sub-parallel	Deep lake	
	Medium	Medium	Poor	Disorder	Shallow lake	
	Medium	Medium-strong	Medium-high	Parallel	Braid river delta	
	Medium	Medium	Poor	Sub-parallel-disorder	Delta plain	
Filling seismic facies	Medium	Medium	Low-medium	Foreset	Delta front	
Wedge seismic facies	Medium-low	Medium-weak	Low-poor	Disorder-foreset	Fan delta	
	Medium-low	Weak	Poor	Disorder	Sub-water fan	
Block seismic facies	Low	Medium-weak	Poor	Sub-parallel-disorder	Flood plain	
Mound seismic facies	Medium	Medium	Medium	Sub-parallel	Fan delta Sub-water fan Braid river delta	

Fig. 4 Correlation of seismic facies to sedimentary facies. The seismic properties refer to the areas bounded by *dotted lines*

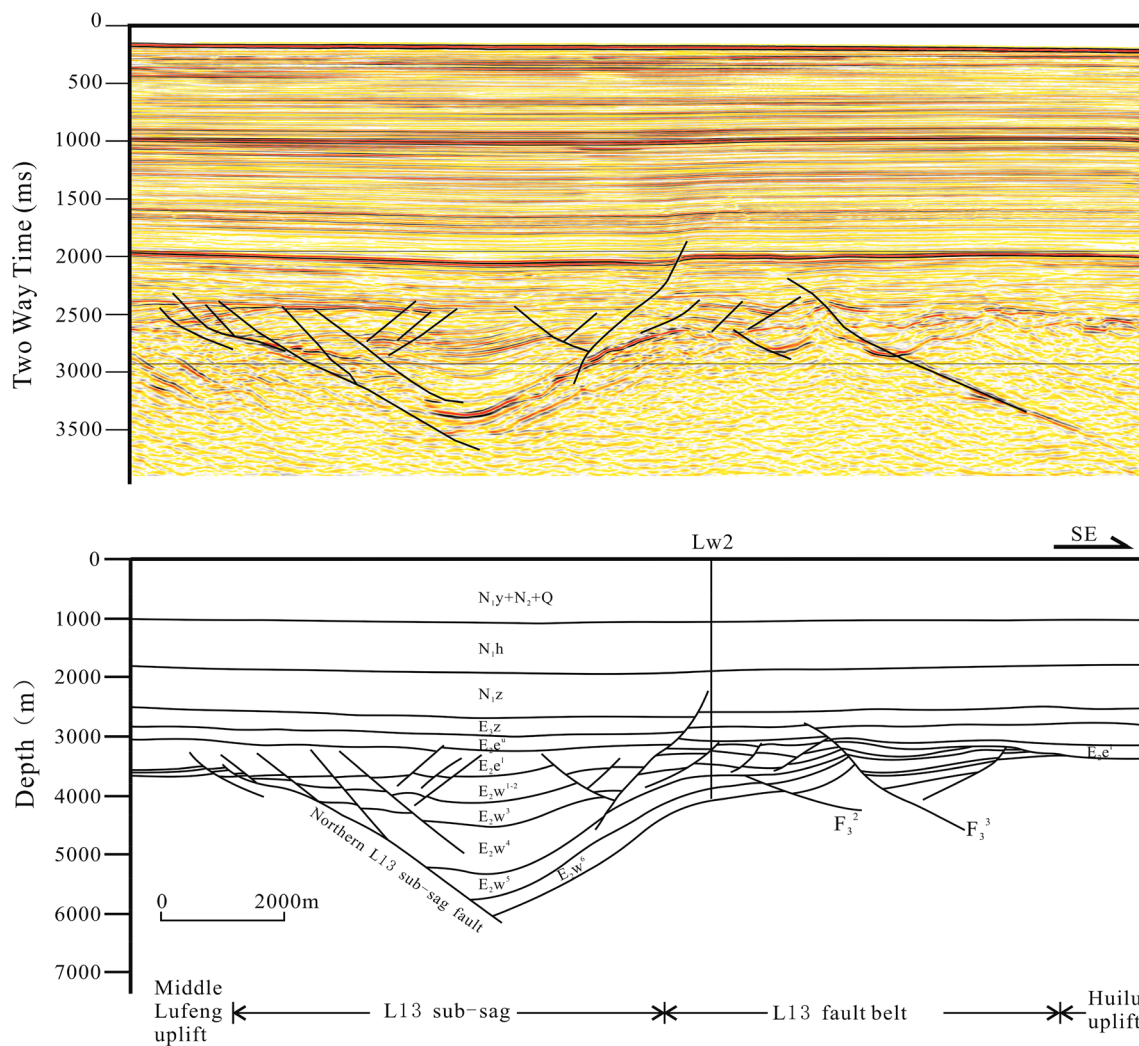


Fig. 5 L1 Seismic profile (*upper*) and geological interpretation (*Lower*). See Fig. 1c for the location

faults slightly deviate from those of the T fractures, based on Fig. 10b. They are oblique normal faults. The eastern part of the northern L13 sub-sag fault (F_1) is oriented NE, and should be the R shears.

A distributed shear model is shown in Fig. 10b (An and Sammis 1996), and distributed shear usually occurs above broad strike-slip zones in basements. This causes distributed shear deformation in the overlying competent sedimentary layers. The model has been used to explain large strike-slip faults such as the San Andres Fault (Miller 1998) and the Australia–Indonesia shear zone (Stevens et al. 2002). The dynamic mechanism of the Riedel shear model in Fig. 10b will be discussed in the section on the basin dynamics.

En echelon faults

En echelon faults are important characteristics of wrench belts (Riedel 1929; Tchalenko 1970; Cunningham and Mann

2007). The geometries of step-over zones and linking faults control contractional or extensional deformation according to the sense of slip and stepping direction of the en echelon fault segments.

Throughout the Zhu-1 depression, the faults are short and display en echelon fashion (Sun et al. 2007; Wu et al. 2015). NE–NEE-striking faults prevail, and NWW striking faults are scarce (Wu et al. 2015). The boundaries between the uplifts and sags (Fig. 3) are composed of NWW and NEE striking faults and slopes. The NWW faults should be T fractures. The NEE striking faults compose en echelon fault belts with NW axes, indicating a left-handed wrench. The wrench should be related to the R’ shears. The other NEE striking faults compose en echelon fault belts with NE axes, indicating a NE right-handed wrench. The wrench should be related to the R shears.

In the L13–L15 sub-sag area, several en echelon fault belts (Fig. 1c) occur with oblique faults with normal

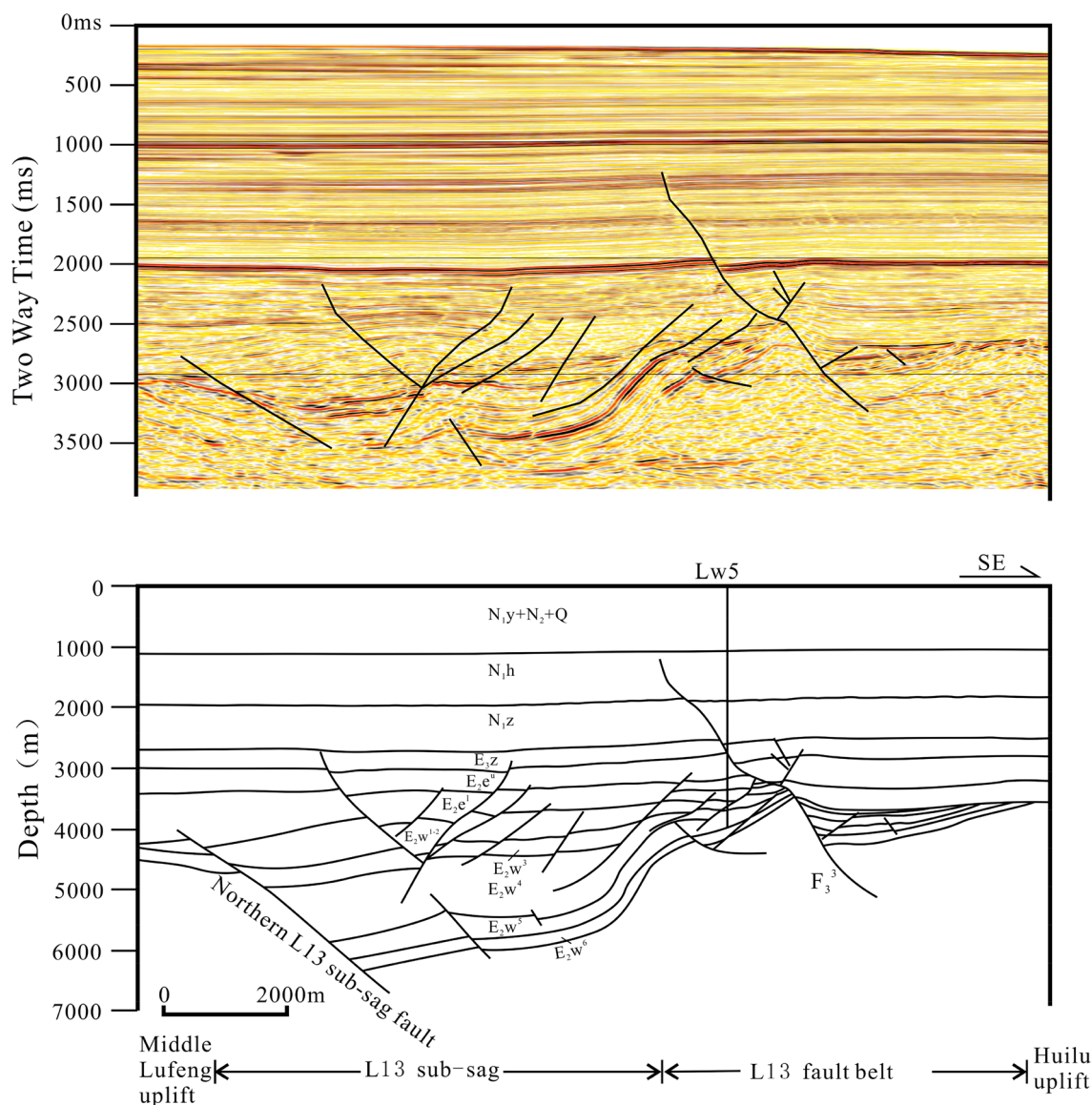


Fig. 6 L2 Seismic profile (*upper*) and geological interpretation (*Lower*). See Fig. 1c for the location

displacements. The en echelon faults in the southwest of the L13 fault belt show evident normal displacement (Figs. 1c, 11). The strikes of the faults were NEE, and their echelon axes trend NW. The normal faults are secondary T fractures, which were caused by the left-handed R' shears. In the eastern part of the L13 fault belt, NWW normal faults are arrayed in an en echelon fault belt with an echelon axis of NE direction (Figs. 1c, 12, 13). The normal faults should be the T fractures.

Negative flower structures

Many strike-slip fault systems are characterized by faults that converge at depth into a single subvertical

fault and form flower structures. In cross-sections, the displacements are predominantly reverse or normal in type, depending on whether the overall fault geometry is transpressional or transtensional. In areas where strike-slip faults occur in converging crust, or transpression, rocks are faulted upward in a positive flower structure. In areas of strike-slip faulting in diverging crust, or transtension, rocks drop to form negative flower structures.

In the middle of the L13-sub-sag, a negative flower structure is observed (Figs. 1c, 14). The main fault was fault F_{4-1} , the dip angle of which exceeded 60°. It was active from the depositional period of the Wenchang formation to that of the Enping formation. The other faults in the flower structure were active during the depositional

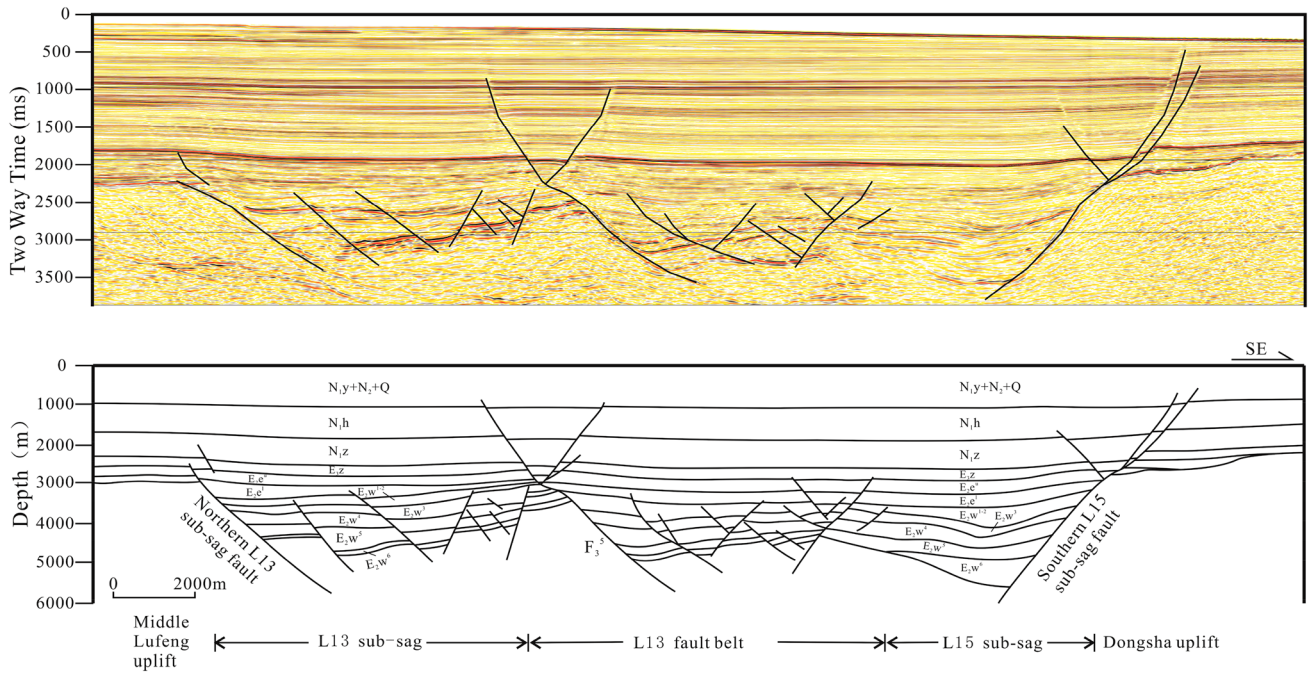


Fig. 7 L3 Seismic profile (*upper*) and geological interpretation (*Lower*). See Fig. 1c for the location

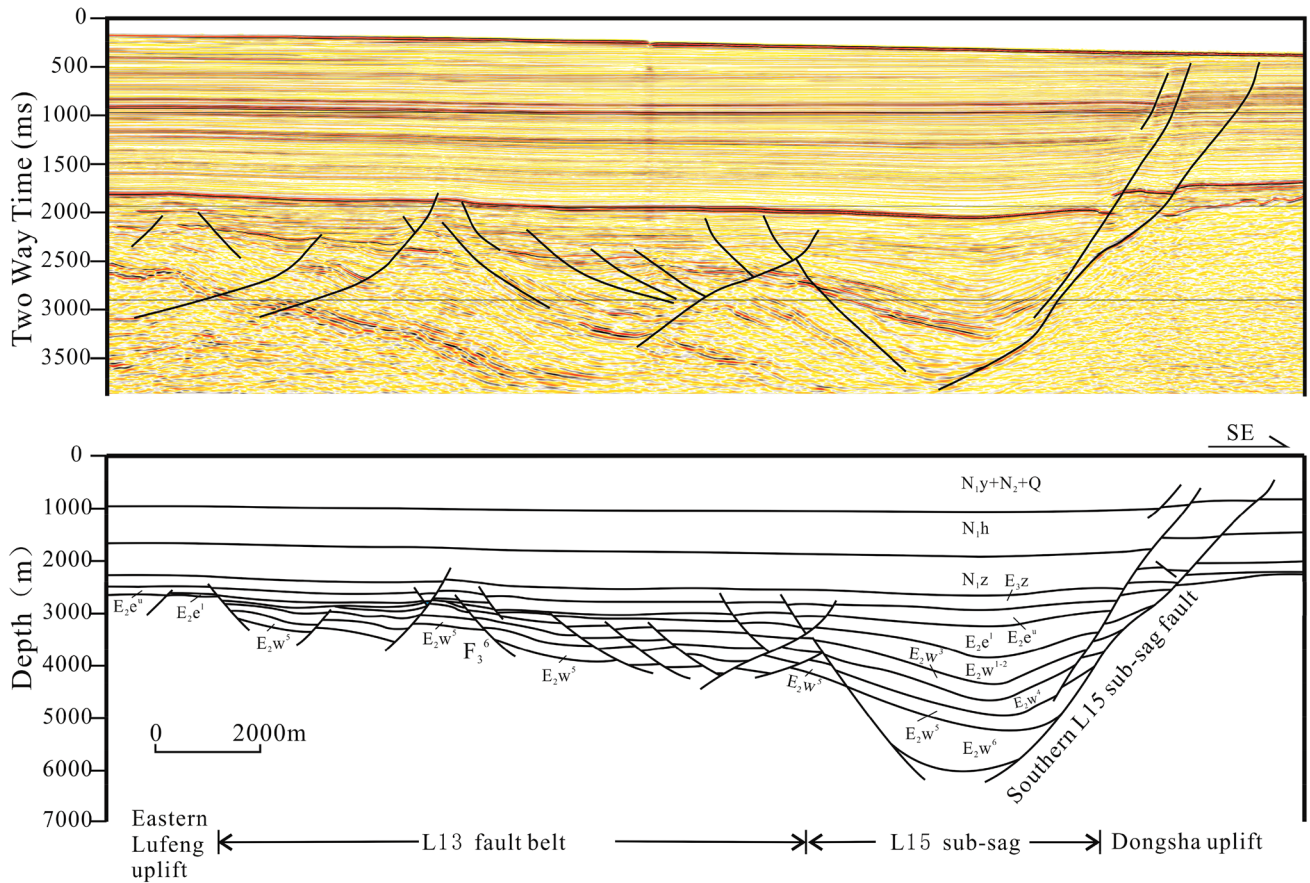


Fig. 8 L4 Seismic profile (*upper*) and geological interpretation (*Lower*). See Fig. 1c for the location

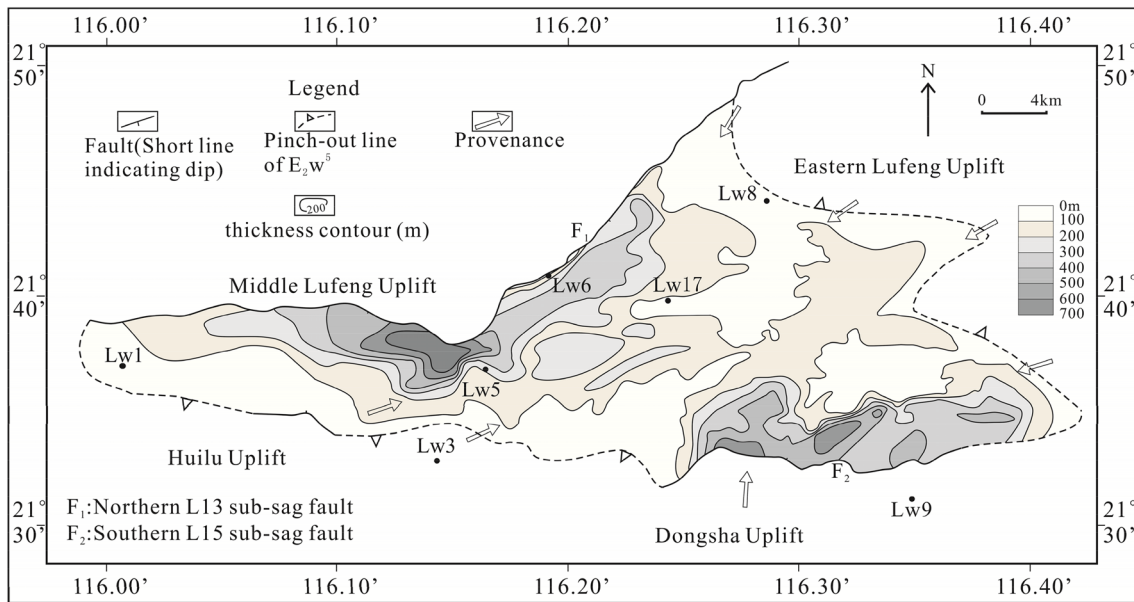
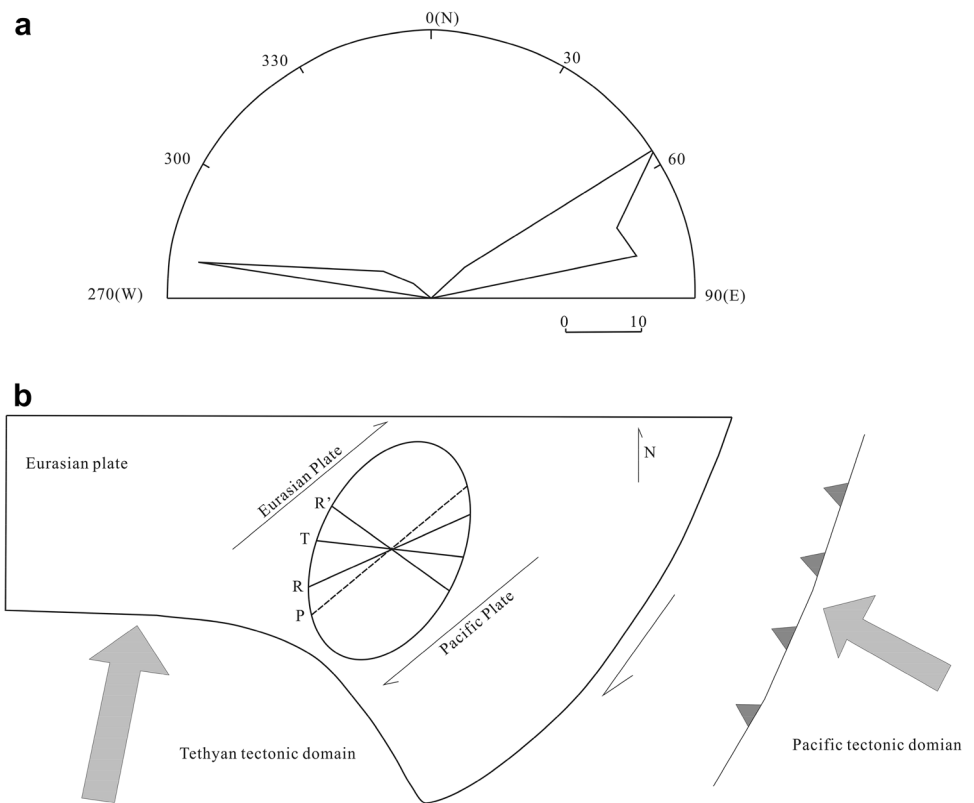


Fig. 9 Thickness contours of the fifth member of the Wenchang formation (E_2w^5). The contours show NWW and NE-NEE directions

Fig. 10 Strike rose diagram of the faults at the base of the Eocene (a) and strain ellipsoid (b) (Modified after Chen et al. 2005)



period of the Wenchang formation to the time of the early deposition of the Enping formation. The faults trend NE and display normal displacements in profiles. They should be the R shears.

Small synclines

The thicknesses of the Wenchang formation (Fig. 3) and the fifth member (Fig. 9) of the Wenchang formation display depocenters or small synclines to the NWW, NEE and NE,

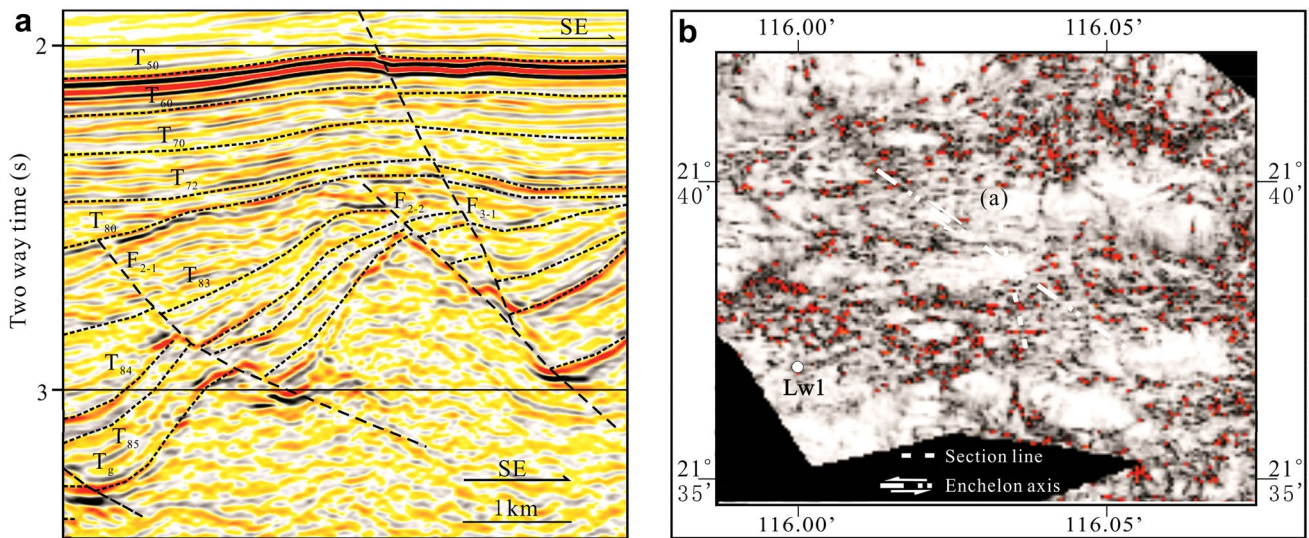


Fig. 11 Profile features (a) and map view (b) of the en echelon faults in the western L13 fault belt (see Fig. 1c for locations and Fig. 2 for connotations of the reflectors). a: seismic profile, b: T_{83} layer-along variance volume slice. The echelon axis in (b) matches that in west of Fig. 1c

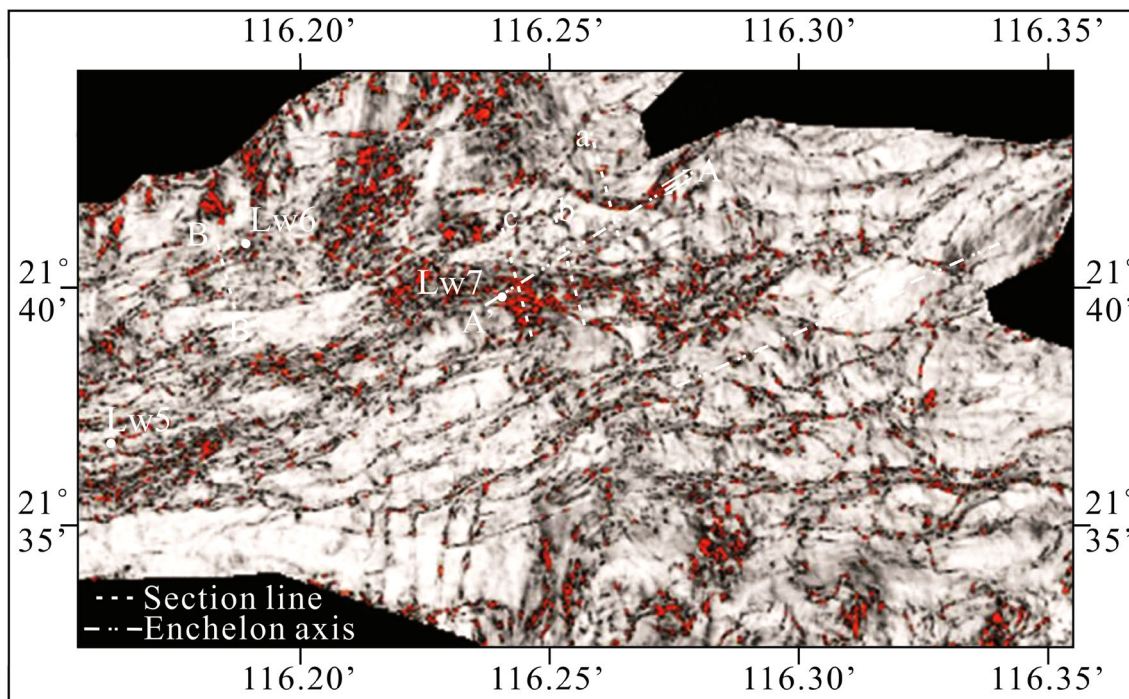


Fig. 12 A T_{83} layer-along variance volume slice in the eastern L13 fault belt. Line BB' matches Line Fig. 14 in Fig. 1c. The two en echelon fault belts match the two belts in Fig. 1c

which indicate the roles of the NE, NEE and NWW faults on deposition. Smaller NE-trending depocenters link to form larger NWW strike-parallel depocenters.

If the extension direction is oblique to the strike of a fault, the shapes of sediment bodies will be syncline with the subsidence centers apart from the main fault. In contrast,

an extensional fault would be accompanied by sedimentary wedge with the thickest strata adjacent to the main fault (Wang et al. 2013). The syncline occurred in the middle segment of the southern fault (F_2) of the L15 sub-sag indicate a transtension (Figs. 1c, 3, 15a). An extension caused by a right-handed wrench would have a NNE direction (Fig. 10b).

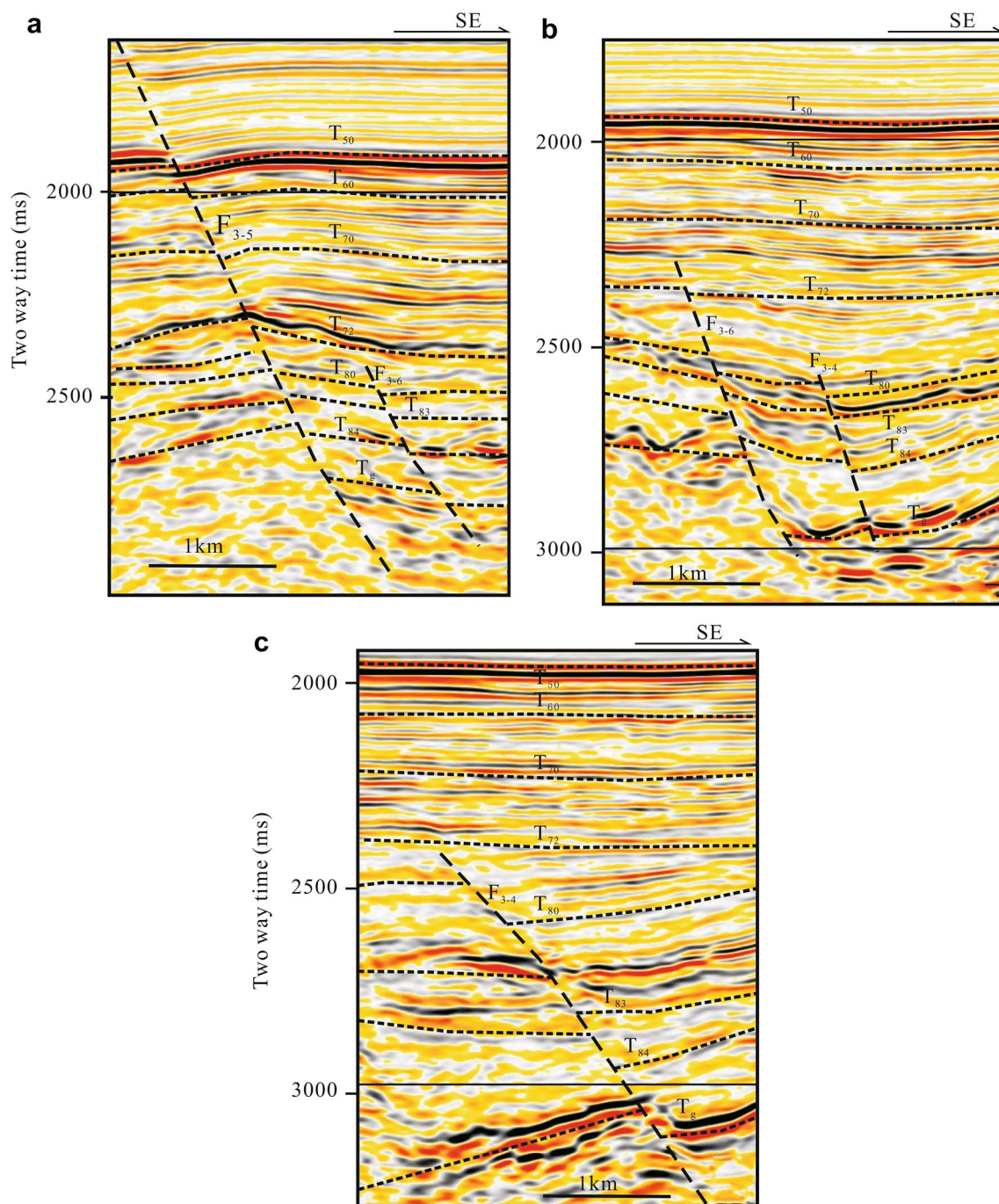


Fig. 13 Profile features of the en echelon faults in the eastern L13 fault belt (see Figs. 1c, 12 for the locations and Fig. 2 for the connotations of the reflectors)

However, the fault segment shown in the syncline in Fig. 14a has a NE strike, because it is a transtensional fault. In the middle segment of the northern L13 sub-sag fault (F_1), the sediment bodies are wedge types, the thickest strata of which are adjacent to the main fault (F_1) (Figs. 1c, 9, 15b). This fault segment is NWW striking, is nearly parallel to the T fractures and is under NNE extension.

Basin evolution and sedimentary history

The L13–L15 sub-sag area began to develop 49 Ma ago during the Middle Eocene. According to the fault growth ratios, shapes of the sedimentary bodies and fault activities, the basin evolution of the PRMB is divided into rifting in the early Eocene, rift-depression transition in the late

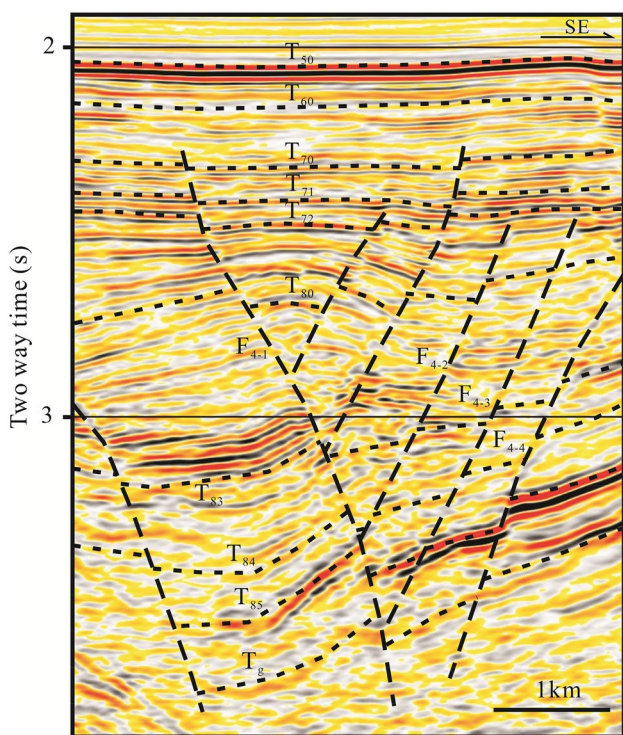


Fig. 14 A negative flower structure in the L13 sub-sag (See Fig. 1c and BB' in Fig. 12 for the locations)

Eocene and post-rift since the Oligocene (Figs. 2, 16). The rift stage comprises three sub-stages: initial rifting in the depositional time of E_2w^6 , intensive rifting in the depositional time of E_2w^5 – E_2w^4 , and late rifting in the depositional time of E_2w^3 – E_2w^1 .

At the initial rifting stage (E_2w^6), small-scale faults were formed (Fig. 16a1, b1), and the extension, which was less than 500 m, was small (Fig. 17). The facies and rocks were

flood plain lithic quartz sandstones and volcanic clastic rocks.

During the intensive rift stage (E_2w^5 – E_2w^4), faulting activity was strong. The faults formed during the deposition of E_2w^6 and extended until they linked; moreover, several newly formed faults appeared within the sub-sags (Fig. 16a2, a3, b2, b3). The extension during the deposition of E_2w^5 increased, and the sedimentary bodies were tabular. The facies of the fifth member (E_2w^5) are meandering river, braid river delta, shore-shallow lake, semi-deep lake and fan delta (Fig. 18). The rocks are lithic quartz sandstones. In the meandering river delta plain, the first set of reservoir sweet spots (Fig. 19) was formed, with a single sand layer thicker than 5 m, a porosity exceeding 8%, and a permeability greater than 1 mD. During the deposition of E_2w^4 , extension or displacement peaked at approximately 1500 m (Fig. 17). The rocks of the fourth member (E_2w^4) are lithic quartz sandstones and mudstones in meandering river delta, fan delta and lake deposits. During the deposition of E_2w^4 , wedge type sedimentary bodies formed and water depth increased. Semi-deep lake mudstones developed. The semi-deep lake mudstones that formed during the deposition of E_2w^4 were the first and most important set of source rocks in the L13–L15 sub sag area and in the PRMB (Zhu et al. 2015). This set of source rocks has an average total organic carbon (TOC) of 0.52%, an average hydrocarbon generating potential ($S_1 + S_2$, sum of residual hydrocarbon in rock and pyrolysed hydrocarbon) of 8.42 mg ((hydrocarbon)/g(rock)), an average reflectance of vitrinite (R_o) of 0.61% and a highest R_o of 0.8%, and it is classified as being at maturation or high maturation. The kerogens are type II₁-I.

During the late rifting stage (E_2w^3 – E_2w^1), faulting activity was weak. The antithetic faults formed, and the L13 sub-sag showed a graben. The L15 sub-sag was still a half-graben with sedimentary wedges (Fig. 15a4, b4). The facies

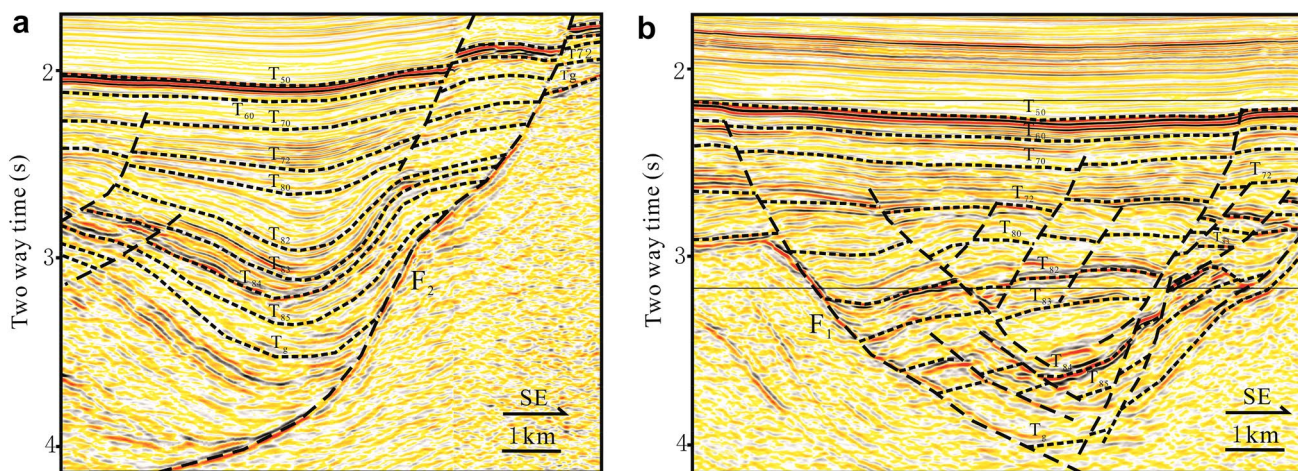


Fig. 15 Two relationships of depocenters to main faults (see Fig. 1c for the locations and Fig. 2 for the connotations of the reflectors)

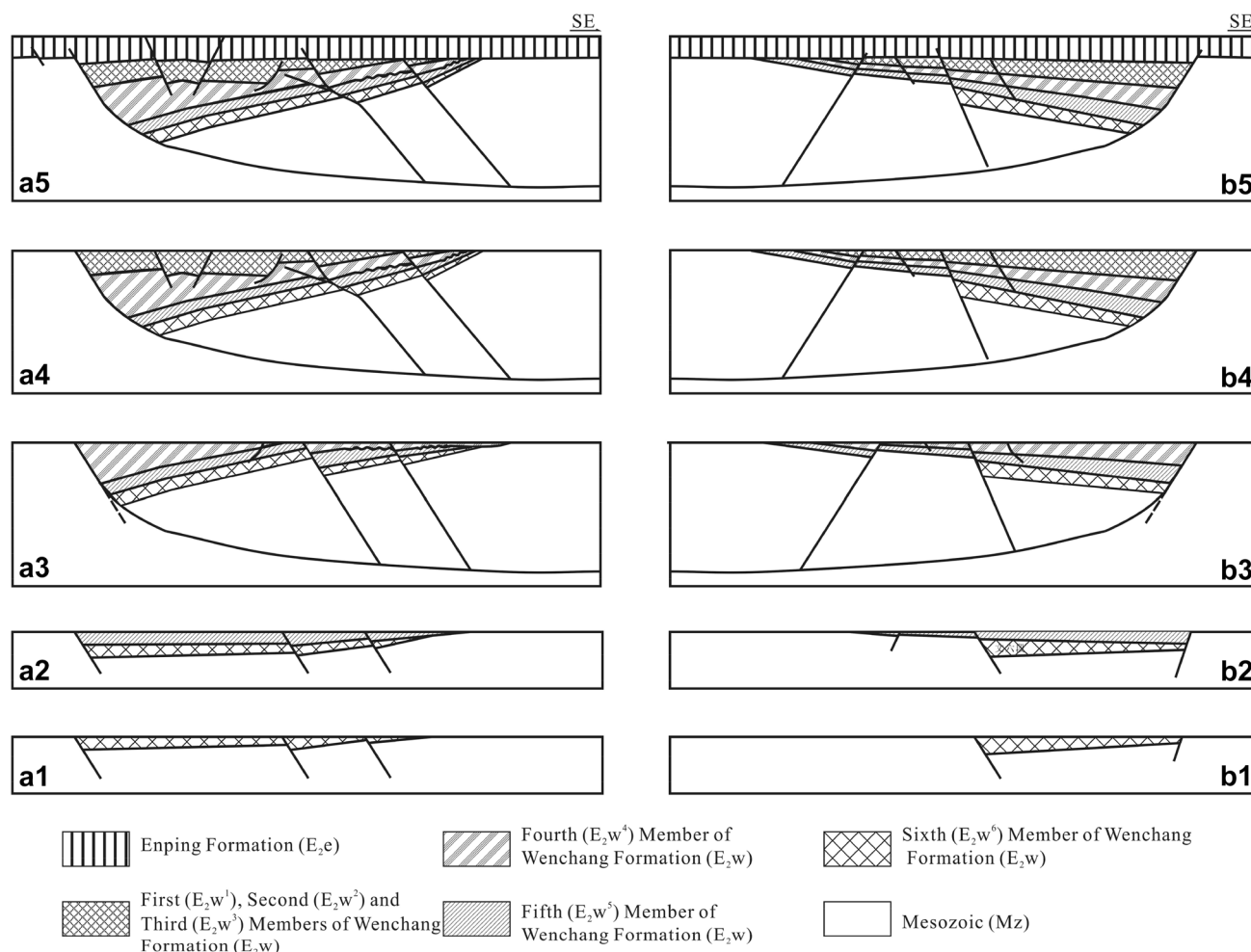


Fig. 16 Schematic of the evolutions of the L13 sub-sag (a, left) and L15 sub-sag (b, right) during the Eocene. (a1–b1): initial rifting; syndimentary faults were formed with thicker beds near the faults. (a2–a3) and (b2–b3): intensive rifting; fast-moving preexisting faults

continued to be active and new faults formed in the inner basin; the bed tilts ranged from 20° to 30°. (a4–b4): late rifting; fault activity decreased and, as a result, the newly deposited beds were gently tilted. (a5–b5): rift-depression transition stage

of the third (E_2w^3), second (E_2w^2) and first (E_2w^1) members were similar to those of flood fans, braid river deltas, shore-shallow lakes and fan deltas. The rocks were feldspathic quartz sandstone, quartz sandstone and mudstone. The lower part of the second set of source rocks, which include the third and second members (E_2w^{3-1}) of the Wenchang formation and Enping formation (E_2e) shallow lake mudstones, was formed. This set of source rocks is composed of type II₂–III kerogen and has a low maturation. Meanwhile, the second set of reservoir sweet spots was formed in the third member (E_2w^3) of the Wenchang formation.

During the depositional period of the Enping Formation, the sediments were tabular bodies with weak fault activity, and the basin transitioned from a rift basin to the post-rift stage (thermal depression stage). Flood fan, meandering river delta, braid river delta and shore-shallow

lake facies comprised the lower section (E_2e^l). The lower section of E_2e^l contained abundant fine grain meandering river delta sediments, and the upper section of E_2e^l was composed of grass grain meandering river delta sediments. Meandering river delta, braid river delta and shallow lake facies comprised the upper section (E_2e^u). The lower section of E_2e^u contains coarse grain meandering river delta sediments, and the upper section of E_2e^u is composed of fine grain meandering river delta and shore-shallow lake sediments (Fig. 20). The rocks in E_2e were feldspathic quartz sandstone, quartz sandstone and mudstone. The shallow lake mudstone of E_2e was formed as the upper part of the second set of source rocks. As a whole, the Enping formation is rich in sandstones, making it a prime candidate for reservoirs.

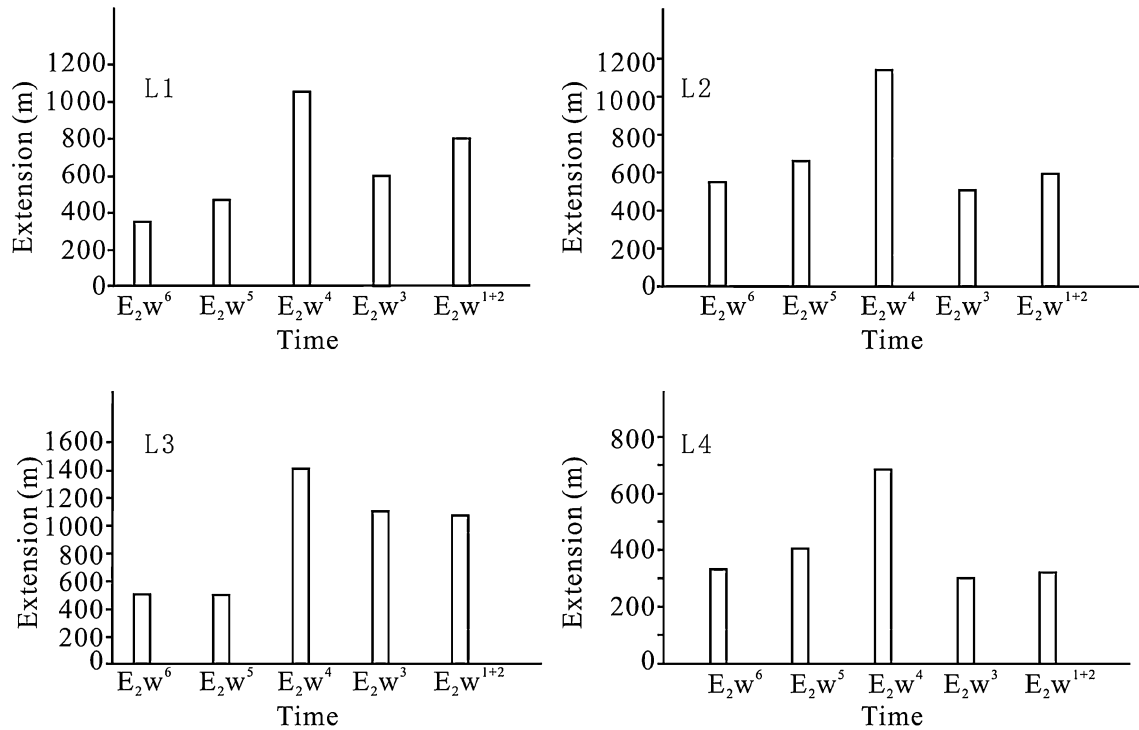


Fig. 17 Horizontal extension in the L13–L15 sub-sag area in the depositional period of the Wenchang formation (E_2w). See Fig. 1c for the locations

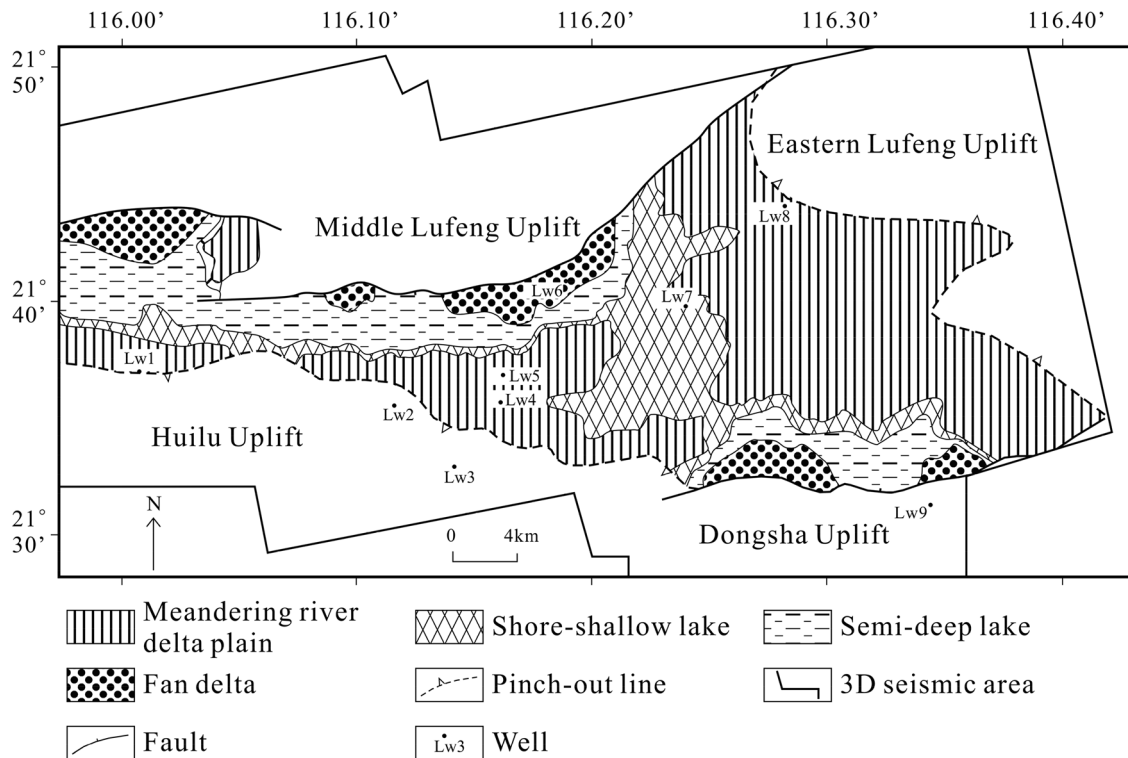


Fig. 18 Sedimentary facies of the fifth member (E_2w^5) of the Wenchang formation

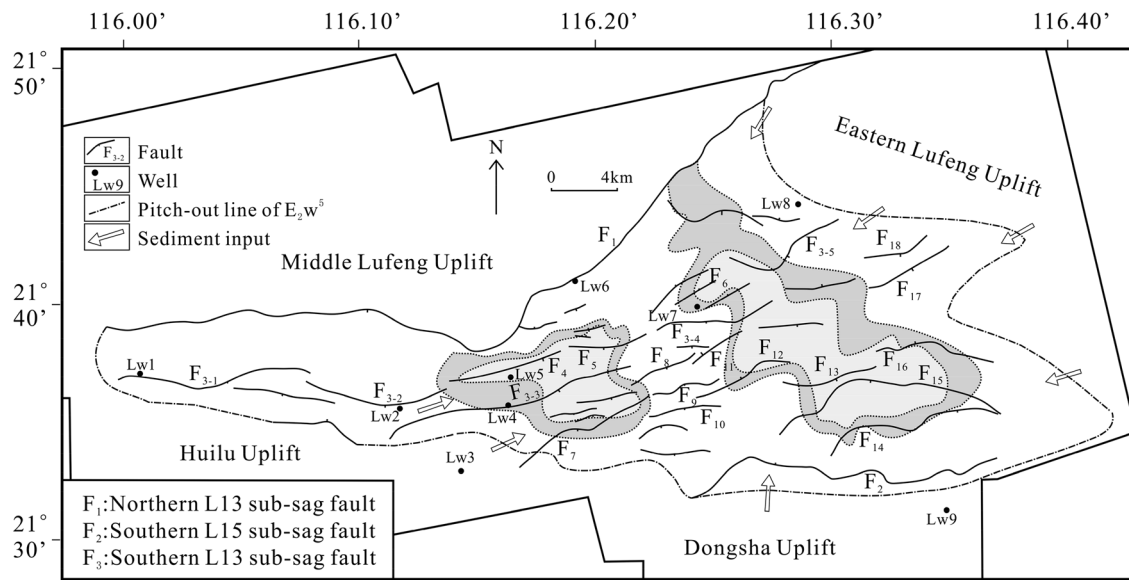


Fig. 19 Distribution of reservoir sweet spots in the fifth member (E_2w^5) of the Wenchang formation

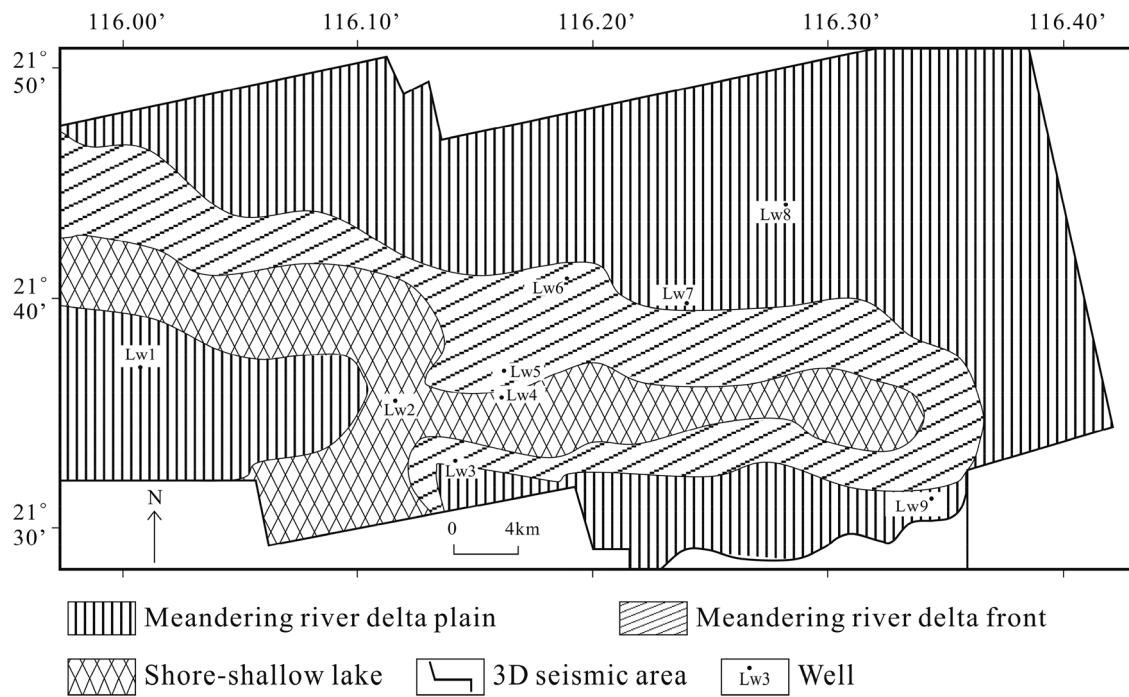


Fig. 20 Sedimentary facies of the upper Enping formation (E_2e^4)

Tectonic controls on deposition

There are clear relationships between the tectonics and deposition in the L13–L15 sub-sag area. The tectonic evolutionary stages have controlled the occurrences of the source rocks and reservoirs. Structures and paleotopography controlled the spatial distribution of the reservoirs.

First, basin evolution and fault activity have controlled the deposition of both the source rocks and the reservoirs. The source rocks formed in the rift stage. The source rock with the most potential for oil generation in the PRMB was formed in the late period of the intensive rifting stage. Reservoir sweet spots were formed in the early period of the intensive rifting stage and in the late rifting stage.

Good reservoirs developed in the rift-depression transitional stage.

In map view, the occurrence of the reservoir sweet spots in E_2w^5 (Figs. 18, 19) indicates that two factors were favorable to their creation. The first is that the fronts of the meandering river delta plain are ideal places for reservoir sweet spots. The second is that the fault steps are also ideal places for reservoir sweet spots. It is therefore clear that the junction sites between the fronts and the fault steps are favorable places for finding reservoir sweet spots. The reservoirs in the Enping formation are distributed along the meandering river delta front and the shore-shallow lake.

Discussion on basin dynamics

There are at least four viewpoints regarding the dynamics of the Pearl River Mouth Basin: those of a northwest-southeast extensional basin (Zhou et al. 1995; Wu et al. 2015), a pull-apart basin (Xu et al. 2004; Li et al. 2012), a right-lateral transtensional basin (Chen et al. 2005) and a left-lateral transtensional basin (Wang et al. 2013). The first and the second mechanisms are unable to explain the combined existence of the NWW-EW and NEE striking faults, the distribution of depocenters and the absence of basin boundary faults in the Zhu-1 depression (Wu et al. 2015). The third mechanism seems reasonable, but the proposed direction of the principal displacement zone would not explain the NWW-EW normal faults or depocenters. The fourth mechanism could explain the faults and the distribution of the depocenters in the Baiyun sag, but it cannot explain the NWW-EW strike normal faults or the distribution of the depocenters in our study area or in the entirety of the Zhu-1 depression.

As described above, in the L13–L15 sub-sag area and throughout the Zhu-1 depression, the fault arrangements in map view, fault features in the profiles, and distribution of depocenters in map view indicate a right-handed wrench (Fig. 10b). Given an inner frictional angle of 30° , a right-lateral wrench in a $NE 52^\circ$ direction, which is the axis of the Zhu-1 depression, would be accompanied by several first order faults including NW 277° trending oblique-normal faults, NW 307° trending R' shears and NE 67° trending R shears. If the secondary faults are considered, the R' shears will cause NE 82° trending faults and the R shears will cause NW 292° trending faults. Therefore, two groups of oblique-normal faults were obtained that had strikes of NW 277° – 292° and NE 82° . The NE 67° R shears display oblique-normal faults because the R shears are transtensional faults (Wu et al. 2009; Xu et al. 2017). Therefore, the faults from the wrench model proposed in this paper match the faults shown in Fig. 10a, including the NWW striking normal faults, NE striking transtensional faults and NEE-EW oblique normal faults.

This specific geo-dynamic can be explained by the plate movements. During the Eocene, the area of the PRMB was part of the Eurasian plate and was located at the southeastern Asian active margin near the South China trench (Honza and Fujioka 2004), to the east of which was the Pacific plate. The Indian-Australian plate was located at the southern part of southeastern Asia. A strong collision occurred between the Indian and Eurasian plates during the Eocene at $45 - 42 \text{ Ma} \pm$ (Lee and Lawver 1995; Xu and Zhang 1999; Chen et al. 2010; Li et al. 2012, 2013). The direction of motion and convergence rate of the Indian–Australian plate with respect to the Eurasian plate were NE 10° – 37° and 4–5.6 cm/a, respectively (Lee and Lawver 1995). On the other hand, the subduction of the Pacific plate with respect to the Eurasian plate was NWW-W and possessed a speed of 30–40 mm/yr during the Eocene (Northrup et al. 1995).

The plate collision in the NE direction and the plate subduction in the NWW direction caused a right-handed wrench in the PRMB area. That right-handed wrench acted on a NE 52° strike, pre-existing basement fault (Fig. 10b). That basement fault is indicated in the Bouguer gravity anomaly and magnetic anomaly maps of the Northern South China Sea and it was formed in the Mesozoic (Chen et al. 2005; Lu et al. 2001; Wang et al. 2013). The fault is called the Qiongdongnan fault (Li et al. 2012) or Yuedong fault (Xu and Zhang 1999). The strike of the basement fault agrees with the strike of the axis of the Zhu-1 depression. Under the right-handed wrench, some NW striking basement faults moved in a left-handed manner, forming sags such as the Baiyun (Wang et al. 2013).

During the Oligocene, the convergence rate between the Eurasian and Pacific plates increased up to 77–90 mm/yr (Northrup et al. 1995). The convergence rate between the Eurasian and Indian–Australian plates remained constant at 40–56 mm/yr (Northrup et al. 1995). The PRMB entered the thermal depression stage.

Conclusions

The faults in the study area have the following characteristics.

- A rose diagram of the fault orientations reveals three peak orientations: NE 56° , NE 77° and NW 277° .
- En echelon faults exist, mainly as NE-NEE faults in the study area.
- Negative flower structures are observed, indicating transtensional fault activity.
- The distributions of the depocenters along the strike-slip faults and normal fault differ in the study area.

Based on the above data, we proposed that the structures in the study area formed due to a right-handed wrench. The L13–L15 sub-sag area underwent a rifting stage in the early Eocene (E_2w) and a rift-depression transition (E_2e) and post-rifting (thermal depression) stage from the Oligocene on. The T normal faults and the R' and R shears and their related secondary normal faults composed the fault systems in the L13–L15 area, indeed, throughout the entire Zhu-1 depression. The right-handed wrench was caused by the collision of the Indian and Eurasian plates.

The tectonic evolution controlled the occurrences of the source rocks and reservoirs. The source rocks with the most potential for oil generation are the deep lake mudstones that developed during the intensive rift stage. Reservoir sweet spots developed in the early part of the intensive rift stage and in the late rifting stage. In map view, the front of the meandering river delta plain and the fault steps are potential places for reservoir sweet spots. In consequence, the junction sites between the fronts and steps are most likely to have reservoir sweet spots. Good reservoirs prevailed in the rift-depression transitional stage.

Acknowledgements This study was supported financially by the National Natural Science Foundation of China (Grant No. 41172124) and the Shenzhen Branch, CNOOC (China) Co., Ltd. The authors would like to thank Langbo Jia from the China University of Petroleum, Beijing, and Zhen Yi from the Shenzhen Branch for their help in the preparation of this manuscript. The helpful comments from the three anonymous reviewers are gratefully acknowledged.

References

- Allen PA, Allen JR (2013) Basin analysis-principles and application to petroleum play assessment. Wiley, Oxford
- An LJ, Sammis CG (1996) Development of strike-slip faults: shear experiments in granular materials and clay using a new technique. *J Struct Geol* 18:1061–1077
- Chen HZ, Wu XJ, Zhou D, Wang WY, Hao HJ (2005) Meso-Cenozoic faults in Zhujiang River Mouth basin and their geodynamic background. *J Trop Oceanogr* 24:52–61
- Chen SP, Zhou XH, Tang LJ, Wang YB, Lu DY, Sun MS, Qu DM (2010) Wrench-related folding: a case study of Bohai Sea basin, China. *Mar Pet Geol* 27:179–190
- Cho N, Martin CD, Sego DC (2008) Development of a shear zone in brittle rock subjected to direct shear. *Int J Rock Mech Min* 45:1335–1346
- Cunningham W, Mann P (2007). Tectonics of strike-slip restraining and releasing bends. *Geol Soc Lond Special Pub* 290:1–12
- Davis GH, Bump AP, Garcia PE, Ahlgren SG (2000) Conjugate Riedel deformation band shear zones. *J Struct Geol* 22:169–190
- Honza E, Fujioka K (2004) Formation of arcs and backarc basins inferred from the tectonic evolution of southeast Asia since the late Cretaceous. *Tectonophysics* 384:23–53
- Lee TY, Lawver LA (1995) Cenozoic plate reconstruction of Southeast Asia. *Tectonophysics* 251:85–138
- Li SZ, Suo YH, Liu X, Dai LM, Yu S, Zhao SJ, Ma Y, Wang XF, Cheng SX, Xue YC, Xiong LJ, An HT (2012) Basic structural pattern and tectonic models of the south China sea: problems, advances and controversies. *Mar Geol Quat Geol* 32:35–53
- Li SZ, Yu S, Zhao SJ, Liu X, Gong SY, Suo YH, Dai LM, Ma Y, Xu LQ, Cao XZ, Wang PC, Sun WJ, Yang Z, Zhu JJ (2013) Tectonic transition and plate reconstructions of the east Asian continental margin. *Mar Geol Quat Geol* 33:65–94
- Lu BL, Wang PJ, Zhang GC, Zhang B, Sun XM, Li WZ, Lang YQ (2001) Basement structures of an epicontinental basin in the northern South China Sea and their significance in petroleum prospect. *Acta Petrolei Sinica* 32:580–587
- Miller DD (1998) Distributed shear, rotation, and partitioned strain along the San Andreas fault, central California. *Geology* 26:867–870
- Moore DE, Byerlee J (1992) Relationships between sliding behavior and internal geometry of laboratory fault zones and some creeping and locked strike-slip faults of California. *Tectonophysics* 211:305–316
- Northrup CJ, Royden LH, Burchfiel BC (1995) Motion of the Pacific plate relative to Eurasia and its potential relation to Cenozoic extension along the eastern margin of Eurasia. *Geology* 23:719–722
- Riedel W (1929) Zur mechanik geologischer brucherscheinungen. *Zentralblatt für Mineralogie. Geol und Pal B* 8:354–368
- Rowan MG, Kligfield R (1989) Cross-section restoration and balancing as aid to seismic interpretation in extensional terranes. *AAPG Bull* 73:955–966
- Shi HS (2013) On heterogeneous distribution and differential enrichment by zones of hydrocarbon resources: a case in Zhu-I depression, Pearl River Mouth basin. *China Offshore Oil Gas* 25:1–25
- Shi HS, Zhu JZ, Jiang ZL, Shu Y, Xie TJ, Wu JY (2009) Hydrocarbon resources reassessment in Zhu I depression, Pearl River Mouth basin. *China Offshore Oil Gas* 21:9–14
- Shu Y, Shi HS, Du JY, Lei YC, Zhang XT (2014) Paleogene characteristics in hydrocarbon accumulation and exploration direction in Zhu I depression. *China Offshore Oil Gas* 26:37–42
- Stevens CW, McCaffrey R, Bock Y, Genrich JF, Pubellier M, Subarya C (2002) Evidence for block rotations and basal shear in the world's fastest slipping continental shear zone in NW New Guinea. In: S. Stein and J. T. Freymueller (eds) Plate boundary zones, *Geodyn. Ser.*, vol. 30, AGU, Washington, D. C, pp. 87–99
- Sun LT, Chen CM, Zhan WH, Shen J, Liu BJ, Wu XJ (2007) Characteristics and influencing factors of fault sealing in Pearl River Mouth basin. *Acta Petrolei Sinica* 28:36–40
- Sun XM, Zhang XQ, Zhang GC, Lu BL, Yue JP, Zhang B (2014) Texture and tectonic attribute of Cenozoic basin basement in the northern South China Sea. *Sci China Earth Sci* 57:1199–1211
- Tchalenko JS (1970) Similarities between shear zones of different magnitudes. *GSA Bull* 81:1625–1640
- Tearpock DJ, Bischke RE (1991) Applied subsurface geological mapping. Prentice-Hall, Englewood Cliffs
- Twiss RJ, Moores EM (2007) Structural geology. W.H. Freeman and Company
- Wang JH, Pang X, Tang DQ, Liu BJ, Xu DH (2013) Transtensional tectonism and its effects on the distribution of sandbodies in the Paleogene Baiyun Sag, Pearl River Mouth basin, China. *Mar Geophys Res* 34:195–207
- Wu JE, McClay K, Whitehouse P, Dooley T (2009) 4D analogue modelling of transtensional pull-apart basins. *Mar Petrol Geol* 26:1608–1623
- Wu ZP, Hu Y, Zhong ZH (2015) Cenozoic faults characteristics and regional dynamic background. *J Chin Petrol Univ* 39:1–9
- Xu JY, Zhang LY (1999) Genesis of Cenozoic basin in the eastern margin of Eurasia plate: dextral pulling—apart. *Oil Gas Geol* 20:187–191
- Xu JY, Yang WR, Zeng ZX, Ben-Avraham Z, Lee TY, Li ZL, Basile C, Zhang LY (2004) Genesis of South China Sea : intervening

- of dextral pull-apart and sinistral transpression. *Earth Sci Front* 11:193–206
- Xu SS, Peng H, Nieto-Samaniego AF, Chen SP, Wu XD (2017) The similarity between Riedel shear patterns and strike-slip basin. *Geol Rev* 63:287–301
- Yang JM (2000) Natural gas resources offshore China. *China Offshore Oil Gas* 14:300–305
- Zhou D, Ke R, Chen HZ (1995) Kinematics of Cenozoic extension on the South China Sea continental margin and its implications for the tectonic evolution. *Tectonophysics* 251:161–177
- Zhou XH, Shi H, Sun SB, Li JY, Liu ML (2006) Application of comprehensive seismic attributes analysis in prediction of Archaean metamorphic rock buried-hill reservoir in JZS oil/gas field. *Oil Geophys Prospect* 41:541–545
- Zhu JZ, Shi HS, Long ZL, Du JY, Shu Y, Shi Y (2015) Accumulation pattern and hydrocarbon distribution of half-graben accumulation system in Zhuyi depression. *Chin Petrol Explor* 20:24–37